Journal of Neuroscience Methods 136 (2004) 111–121

JOURNAL OF NEUROSCIENCE METHODS

www.elsevier.com/locate/jneumeth

An algorithm for real-time extraction of population EPSP and population spike amplitudes from hippocampal field potential recordings

Ghassan Gholmieh [a], Spiros Courellis [a,*], Angelika Dimoka [a], Jack D. Wills [c], Jeff LaCoss [c], John J. Granacki [a,c,d], Vasilis Marmarelis [a], Theodore Berger [a,b]

[a] *Department of Biomedical Engineering, University of South Carolina, Los Angeles, CA 90089-1451, USA*
[b] *Neuroscience Program, USC, Los Angeles, CA 90089-2520, USA*
[c] *Information Sciences Institute, University of Southern California, Los Angeles, CA 90089, USA*
[d] *Department of Electrical Engineering, University of Southern California, Los Angeles, CA 90089, USA*

Received 20 March 2003; received in revised form 7 January 2004; accepted 9 January 2004

Abstract

A new method is presented for extracting the amplitude of excitatory post synaptic potentials (EPSPs) and spikes in real time. It includes a low pass filter (LPF), a differentiator, a threshold function, and an intelligent integrator. It was applied to EPSP and population spike data recorded in the Dentate Gyrus and the CA1 hippocampus in vitro. The accuracy of the extraction algorithm was evaluated via the extraction normalized mean square error (eNMSE) and was found to be very high (eNMSE $< 5\%$). The preservation of neuronal information was confirmed using the Volterra–Poisson modeling approach. Volterra–Poisson kernels were computed using amplitudes extracted with both proposed and traditional methods. The accuracy of the computed kernels and the resulting model was evaluated via the prediction normalized mean square error (pNMSE) and was found to be very high (pNMSE $< 5\%$). The similarity between the kernels computed when the proposed method was used to extract the field potential amplitude and their counterparts when the traditional method was used to extract the field potential amplitude confirms the preservation of the neuronal dynamics. The proposed method represents a new class of real time field potential amplitude extraction algorithms with complexity that can be included in hardware implementations.

Keywords: CA1; Dentate Gyrus; EPSP; Nonlinear analysis; Random train; Spike amplitude; Short-term plasticity; SoC

1. Introduction

Real time extraction and monitoring of the amplitude of evoked field potentials is important in neurosurgery (Colletti et al., 1997; Stecker et al., 1996; Zaaroor et al., 1993), biosensor applications (Gholmieh et al., 2001; Stoppini et al., 1997; Thiebaud et al., 1997), and the design of neural prosthetics (Donoghue, 2002; Pesaran et al., 2002). Current experimental methods for measuring the amplitude of evoked potentials (e.g. excitatory post synaptic potentials (EPSPs) and population spikes (PSs)) are based on software algorithms that are difficult to implement in hardware. In this article, we have introduced an algorithm for real time field potential amplitude extraction that can be incorporated in hardware implementations. The proposed algorithm was motivated by the design of a novel cortical neuroprosthetic (Berger et al., 2001) that requires as input the values of field potential amplitudes in real time and generates the corresponding output based on a hardware implementation of a Volterra–Poisson model that represents the functionality implemented by the neuroprosthetic device.

Classically, the amplitude of the EPSP waveform is defined as the maximum positive value from the baseline (Fig. 1A) and the amplitude of the population spike as the distance between the minimum and the point that corresponds to the projection of the minimum on the line joining the two positive peaks (Fig. 1B) (Johnston and Daniel, 1995; Lagmoen and Andersen, 1981). Typically the EPSP amplitude is computed using minimax-based algorithms. Similarly, the computation of the population

* Corresponding author. Tel.: +1-213-740-0340; fax: +1-213-740-0343.
E-mail address: shc@usc.edu (S. Courellis).

0165-0270/$ – see front matter © 2004 Elsevier B.V. All rights reserved.
doi:10.1016/j.jneumeth.2004.01.006

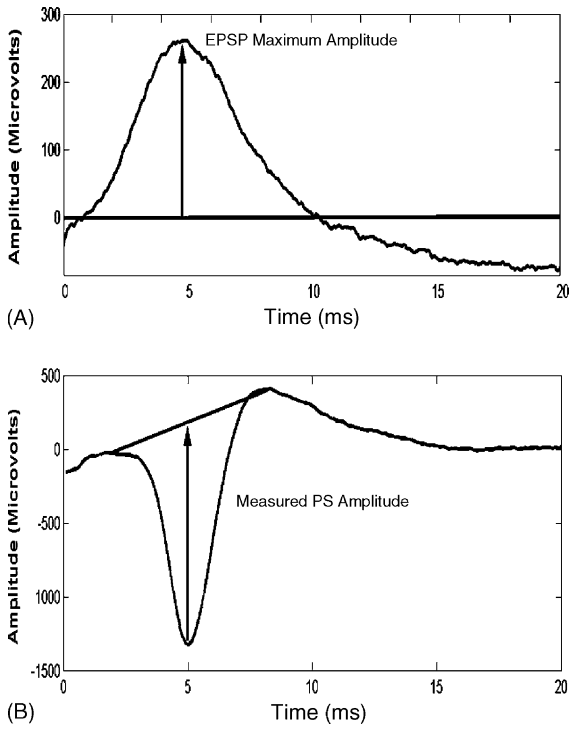

Fig. 1. (A) Classic EPSP amplitude extraction. The amplitude of the EPSP waveform is evaluated by getting the maximum value. (B) Classic PS amplitude extraction. The population spike amplitude is measured by taking the distance between the negative minimum and the point that corresponds to the projection of the minimum on the line joining the two positive peaks.

spike amplitude involves a number of heuristics to reliably isolate the minimum and the maxima in a typically noisy EPSP. Although software based real time implementations for the extraction of field potential amplitudes have been implemented (Anderson and Collingridge, 2001), the majority of these methods can become cumbersome when it comes to real time hardware implementation in the scale of microseconds.

In this article, we introduce an improved new algorithm for real time extraction of excitatory postsynaptic potential amplitude and population spike amplitude. The proposed algorithm is based on previously introduced methods for spike detection (Hedwig and Knepper, 1992; Marion-Poll and Tobin, 1991). It consists of a low pass filter (LPF), a differentiator, a threshold function, and an intelligent integrator. It was tested using EPSPs and population spikes recorded at the Dentate Gyrus and the CA1 hippocampus in vitro. The amplitudes extracted with the proposed method were compared to the amplitudes obtained through the classical extraction method using the extraction normalized mean square error (eNMSE). The preservation of neuronal information was evaluated via the prediction normalized mean square error (pNMSE) of models derived using the Volterra–Poisson modeling approach (Courellis et al., 2000; Gholmieh et al., 2002).

2. Materials and methods

2.1. Hippocampal slice preparation

Halothane anesthetized adult rats were decapitated. The hippocampus was extracted and bathed in iced aCSF. Transverse slices (400–500 μm in thickness) were collected using a Leika vibratome (VT 1000S) and were left for 2 h in aCSF to recover at room temperature. During the recording phase, slices were maintained submerged using a nylon mesh. This protocol was approved by the Department of Animal Resources and Institutional Animal Care at the University of Southern California. Details on the hippocampal slice preparation can be found in Xie et al. (1992), and Gholmieh et al. (2001).

2.2. Hardware materials

The data were collected using two multielectrode setups, each operated by a different user. The EPSP data were collected using the multielectrode array (MEA) setup, and the

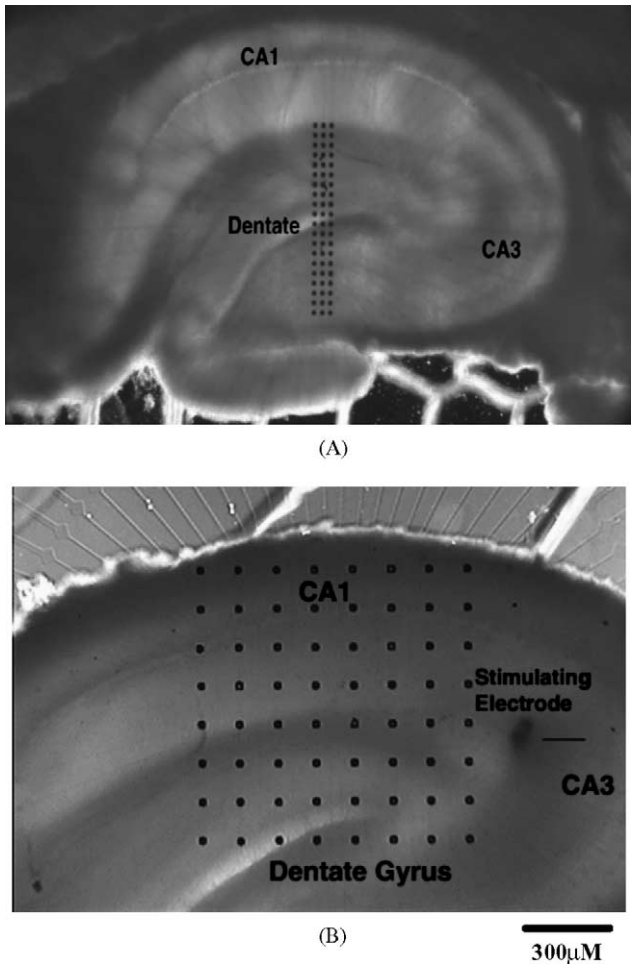

Fig. 2. (A) Acute rat hippocampal slice positioned on the MEA array. (B) Acute rat hippocampal slice positioned on the MMEP array.

PS data were collected using the multi-micro-electrode-plate (MMEP) setup.

2.2.1. MEA setup

The MEA system (www.multichannelsystems.com, Egert et al., 1998) consisted of a 60-electrode array, pre-amps, and data acquisition hardware and software. The electrode array was a custom-built multielectrode array (Han et al., 2002), with the electrodes in a 3×20 arrangement (Fig. 2A). The gold-based electrodes diameter was 30 μm with an inter-electrode distance of 50 μm. The total gain (amplification) was 1200× with a noise level around ±10 μV. Data were sampled at a frequency of 25 kHz per channel with a resolution of 16 bits and were analyzed using MCS software (MCRack v 1.44).

2.2.2. MMEP setup

The MMEP setup consisted of a 64-electrode array arranged into an 8×8 formation (Fig. 2B) [Gross et al., 1993; Univ. North Texas, www.cnns.org], pre-amp, data acquisition boards, and custom-designed software. The recorded signal was amplified in two stages (2500×). The preamp had a gain of 250 while the data acquisition board gain was set at 10. The noise level was around ±20 μV. Data were sampled at a frequency of 7.35 kHz per channel with a resolution of 16 bits. The software for data recording, preprocessing, and analysis was based on custom written Matlab procedures (Gholmieh et al., 2001).

2.3. Data collection

Random impulse trains (RITs) consisting of 400 fixed amplitude impulses with Poisson distributed (mean frequency of 2 Hz) interimpulse intervals were used to stimulate the afferent fibers. The medial Perforant Path (Dentate Gyrus afferents) was stimulated in the range of [50–100 μA] using an adjacent pair of electrodes (biphasic current) and the corresponding EPSP waveforms were recorded from the granular cell layer using the MEA setup. Data were recorded from the channel that had the highest EPSP amplitude, corresponding to an electrode located over the cell body layer of the granule cells.

The Schaffer Collaterals (CA1 afferents) were stimulated in the range of [200–400 μA] using an external bipolar electrode of twisted Nichrome wires (biphasic current) and the corresponding PS waveforms were recorded from the pyramidal cell layer using the MMEP setup. The population spike data were recorded from the channel that had the highest population spike amplitude and the corresponding electrode of which was located over the cell body layer.

2.4. Analytical methods

EPSP and PS amplitudes were extracted with the proposed method and the classical method. The differences were evaluated by computing the extraction normalized mean square error between corresponding datasets processed with the classical method and the proposed method. The preservation of neuronal information was evaluated using the Volterra–Poisson modeling approach. We compared kernels computed with output datasets extracted using the classical method with their counterparts computed with output datasets extracted using the proposed method. The quality of prediction and accuracy of the kernels was evaluated using the prediction NMSE (pNMSE).

2.4.1. Classical amplitude extraction

The EPSP amplitude was computed as the maximum value in the recorded waveform (Fig. 1A). The PS amplitude was measured by finding first the coordinates of the first upward-going (positive) peak, the second upward-going peak, and the in between downward-going (negative) peak

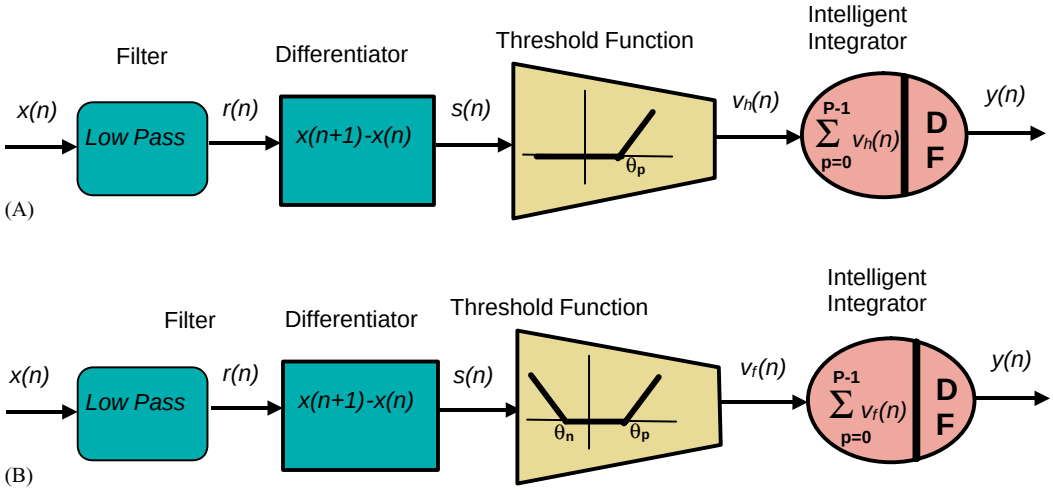

Fig. 3. The amplitude extraction algorithm. The data were processed in series using a low pass filter, a differentiator, a threshold function, and an integrator. (A) EPSP extraction algorithm. (B) PS extraction algorithm.

(Fig. 1B). Then, the spike amplitude was computed as the length of the vertical line drawn from the negative peak to the line joining the two positive peaks (Johnston and Wu, 1995; Lagmoen and Andersen, 1981).

2.4.2. Real time EPSP and PS amplitude extraction

The amplitude extraction mechanism was comprised of a low pass filter, a differentiator, a threshold function, and an intelligent integrator (Fig. 3). The low pass filter attenuated the high frequency noise so as not to be amplified by the differentiator. The selection of the cutoff frequency was based on using the EPSP and PS power spectrum to identify the frequency range of the desirable signal. If $x(n)$ is the digitized input to the LPF filter and $r(n)$ is its output, then:

$$r(n) = \sum_{m=0}^{M-1} h(m) \times (n - m) \tag{1}$$

where $h(m)$ is the impulse response of the filter. In our case, we used a FIR filter of order M with $h(m) = c_m$ the filter coefficients. The coefficients of the FIR filter can be computed using a variety of techniques available in several commercial signal processing packages. Although a digital FIR filter has been used in this study, an analog filter could also be used at the signal conditioning stage before A/D conversion.

A simple differentiator followed the LPF and was used to accentuate rapid varying waveforms in relation to slower varying waveforms. This was particularly useful in the case of a rapid varying spike present in a slower varying EPSP. The operation of the differentiator we used is described by the following equation:

$$s(n) = r(n) - r(n-1), \qquad n > 0 \tag{2}$$

The output $s(n)$ of the differentiator was then fed into a thresholding nonlinearity. The output of the threshold device for the PS and EPSP was:

$$V_e(n) = \begin{cases} 0, & s(n) < \theta_p \\ s(n), & s(n) > \theta_p \end{cases} \tag{3}$$

and

$$V_s(n) = \begin{cases} s(n), & \theta_p < s(n) \\ 0, & \theta_n < s(n) < \theta_p \\ -s(n), & s(n) < \theta_n \end{cases} \tag{4}$$

where V_e is the device output for EPSPs and V_s is the device output for PSs. The threshold values θ_p and θ_n were real numbers ($\theta_n < \theta_p$) and were chosen to form a band for rejecting weak slow activity and the remaining baseline noise. In the EPSP case, the value of θ_p was set higher than the baseline noise level. In the population spike case, the value of θ_n and θ_p were first set higher than any slow activity or noise. Then, the value of θ_n was increased in order to avoid integrating the repolarization phase of the population spike waveform (Fig. 6H).

The intelligent integrator received the output of the threshold device and integrated over a predefined interval that can be preset or determined dynamically. It was comprised of two functions: the integration function and the decision function. The integration function integrated the incoming signal over a predefined interval. The decision function decided whether the value of the integration function corresponded to a real field potential amplitude or it was the result of an erroneous extraction triggered by noise. If the value of integration did not correspond to a real field potential, it was not let through. The decision function can be viewed as quality control and can involve a number of heuristics. In its simplest form, the decision function could be integration over a predefined interval P after a trigger (typically θ_n for the PS and θ_p for the EPSP), expressed as:

$$y(n) = \gamma \sum_{p=0}^{P-1} V_t(t), \qquad t = e, s \tag{5}$$

where γ is a scaling factor computed by averaging the ratio of the amplitude obtained through and the classical method to the amplitude obtained through the proposed method. P is the length of the integration domain.

In this article, in addition to defining an integration domain, we enriched the decision function with a set of heuristics on the duration of the positive and negative phase of the output of the thresholding nonlinearity and the transition interval from the negative phase to the positive phase. In particular, the output of the intelligent integrator was defined as:

$$y_e(n) = \begin{cases} \gamma \sum_{p=0}^{P-1} V_e(e), & \text{if } w_p > \omega_p \\ 0, & \text{otherwise} \end{cases} \tag{6a}$$

for EPSP amplitude extraction and

$$y_s(n) = \begin{cases} \gamma \sum_{p=0}^{P-1} V_s(p), & \text{if } w_n > \omega_n \quad \text{and} \quad w_p > \omega_p \\ & \quad \text{and} \quad w_{tr} > \omega_{tr} \\ 0, & \text{otherwise} \end{cases} \tag{6b}$$

for spike amplitude extraction, where w_n is the duration of continuous negative activity below θ_n, w_p is the duration of continuous positive activity above θ_p, and w_{tr} is the duration of transition region at the output of the threshold device. ω_n, ω_p, and ω_{tr} were positive real numbers (Fig. 4) that were determined experimentally.

This proposed decision function provided the advantage of rejecting undesirable artifacts at the frequency and amplitude range of the EPSP or the spike. In the EPSP case, the output of the intelligent integrator corresponded to the peak EPSP amplitude, while in the spike case, the output of the intelligent integrator corresponded to the average of the distance between the negative peak and the first positive peak and the distance between the negative peak and the second positive peak.

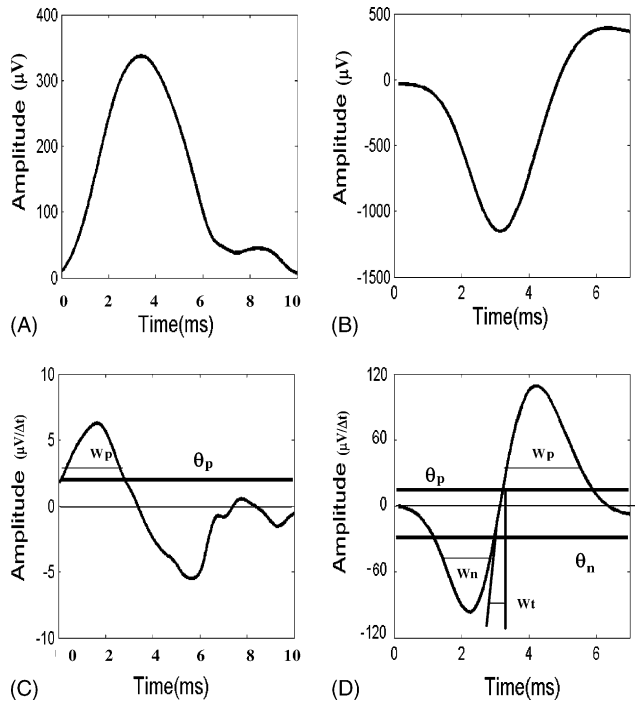

Fig. 4. (A) EPSP waveform. (B) Population spike waveform. *y*-axis: amplitude in microvolts; *x*-axis: time in ms. (C) First order derivative of the EPSP waveform shown in panel. (D) First order derivative of the EPSP waveform shown in panel B. *y*-axis: amplitude in $\mu V/\Delta_t$; *x*-axis: time in ms; w_n is the duration of continuous negative activity; w_p is the duration of continuous positive activity; w_{tr} is the duration of transition region.

The accuracy of the amplitude extraction was evaluated using the extraction normalized mean square error of the amplitude, defined as follows:

$$\text{eNMSE} = \frac{\sum_i (y_{\text{prop}_i} - y_{\text{classical}_i})^2}{\sum_i y^2_{\text{classical}_i}} \quad (7)$$

where y_{prop} is the extracted amplitude of the EPSP or PS using the proposed method, $y_{\text{classical}}$ is the amplitude extracted using the classical method.

2.4.3. Nonlinear dynamics evaluation

The effect of the extraction method on the nonlinear dynamic mapping between the input and the output datasets was assessed using the Volterra–Poisson modeling approach (Courellis et al., 2000; Gholmieh et al., 2002). A second order model was used expressed by the following equation:

$$y(n_i) = k_1 + \sum_{n_i - \mu < n_j < n_i} k_2(n_i - n_j) \quad (8)$$

where n_i is the time of occurrence of the *i*th stimulus impulse, n_j the time of occurrence of the *j*th stimulus impulse prior to the *i*th stimulus impulse, $y(n_i)$ the amplitude of the waveform response to the *i*th stimulus impulse, μ the memory of the biological system, k_1 the first order kernel, and k_2 is the second order kernel. The first order kernel represents the mean of the waveform amplitude of interest while the second order kernel quantifies the effect on the current waveform amplitude of the interaction between the current stimulus impulse and each past stimulus impulse within the memory window μ. The first and second order kernels were calculated using output datasets extracted with the classical ($y_{\text{classical}}$) and the proposed (y_{prop}) method. The accuracy of the computed kernels was evaluated using the normalized mean square error of the predicted amplitude (pNMSE), defined as follows:

$$\text{pNMSE} = \frac{\sum_i (Y_{\text{pr}_i} - Y_{\text{data}_i})^2}{\sum_i Y^2_{\text{data}_i}} \quad (9)$$

where Y_{pr} is the predicted amplitude of the waveform using the computed kernels and Y_{data} is the amplitude extracted from the recorded data using either the classical method or the proposed method. The NMSE is a measure of how well kernels can capture the system nonlinear dynamics. If the NMSE value is small, the kernels model the biological system very well.

3. Results

Two sets of experiments were conducted, each consisting of five experiments. The first set of experiments included EPSP data collected from the Dentate Gyrus in vitro and the second set of experiments included PS data recorded at the CA1 area in vitro. The EPSP and PS amplitudes were extracted using both the classical method and the proposed algorithm. The amplitudes extracted with the proposed method were compared to those obtained by classical method using the extraction normalized mean square error. The preservation of neuronal dynamics was evaluated using the Volterra–Poisson modeling approach. We compared kernels computed with output datasets extracted using the classical method with their counterparts computed with output datasets extracted using the proposed method.

The first step in extracting the EPSP or PS amplitude was low pass filtering. Our implementation of the low pass filter was an FIR filter whose cut-off frequency was determined by the Power spectrum of the EPSP (Fig. 5A) and PS waveform (Fig. 5B). The power spectrum of EPSP data showed a peak between 20 and 40 Hz. The power spectrum of PS data showed three peaks: an early peak between 0 and 10 Hz, a second peak corresponding to the EPSP component between 20 and 40 Hz, and a late peak corresponding to the spike component between 50 and 100 Hz. The values of the power spectrum values became negligible (decreased to less than 0.01) above 300 Hz for the EPSPs and above 400 Hz for the PSs. These frequencies were chosen as the cut-off frequencies for two 30th order FIR filters with 60db attenuation at the cut-off frequency.

Low pass filtering was essential for the amplitude extraction mechanisms. Fig. 6 shows the result of the differentiation of a filtered and unfiltered signal. Fig. 6A shows an unfiltered EPSP waveform and Fig. 6C shows the result of

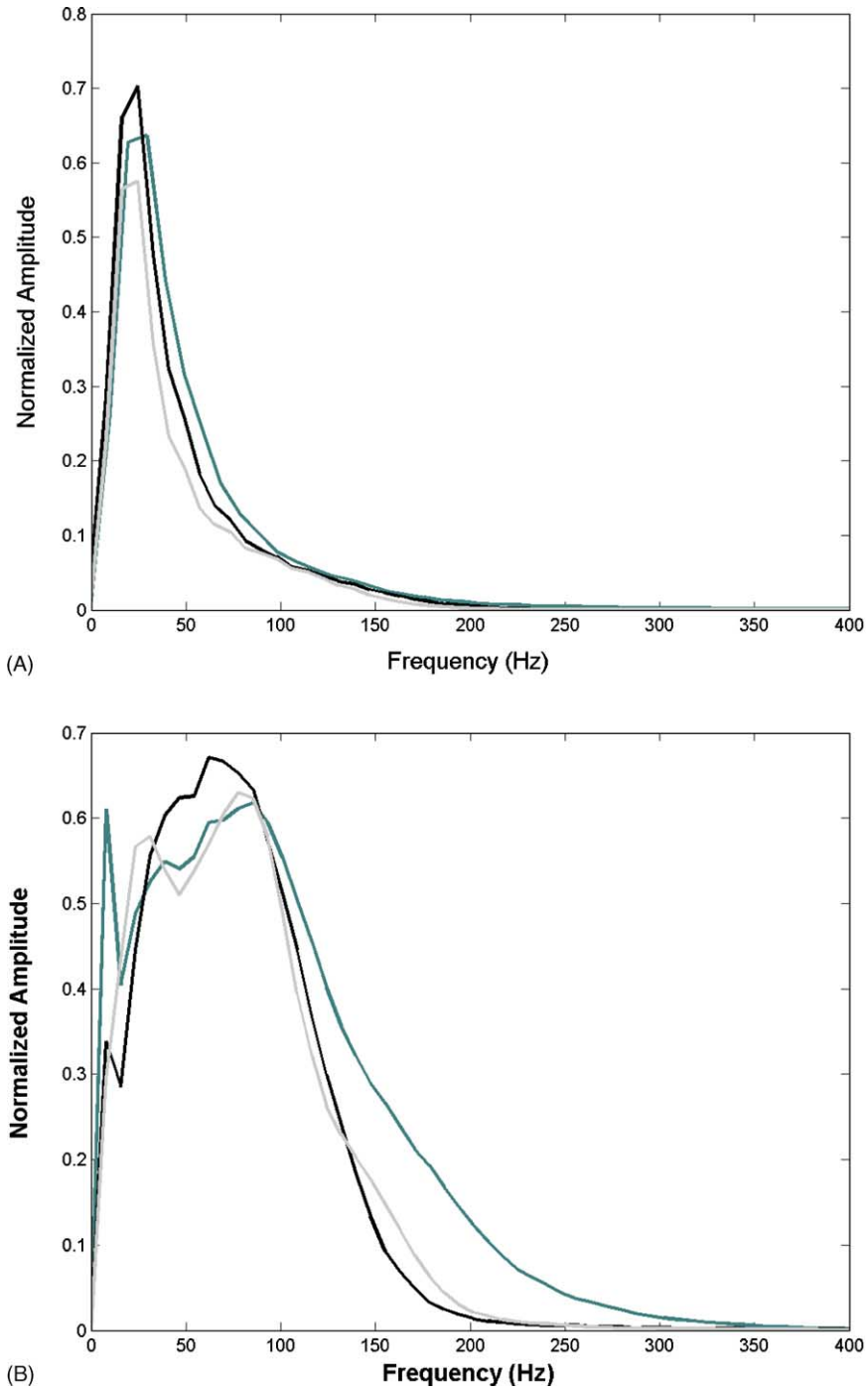

Fig. 5. (A) Power spectrum of EPSP computed from three different experiments. (B) Power spectrum of population spike amplitude also computed from three different experiments.

its differentiation. Fig. 6B shows a filtered EPSP waveform and Fig. 6D shows the result of its differentiation. Comparison between Fig. 6C and Fig. 6D clearly shows the effect of the unfiltered noise on the differentiated signal and illustrates the importance of low pass filtering prior to differentiation. Fig. 6G shows the result of the differentiation of an unfiltered PS (Fig. 6E) while Fig. 6H shows the results of the differentiation of a filtered PS (Fig. 6F). Comparison between Fig. 6G and Fig. 6H confirms the importance of low pass filtering in the case of PS as well.

After low pass filtering, the signal was processed by the simple differentiator and the output of the differentiator was fed into a threshold device. The threshold values were selected to form a band for rejecting weak slow activity and the remaining baseline noise. The value of θ_p in the EPSP case was set at 12.5 μV/ms and the threshold values for the

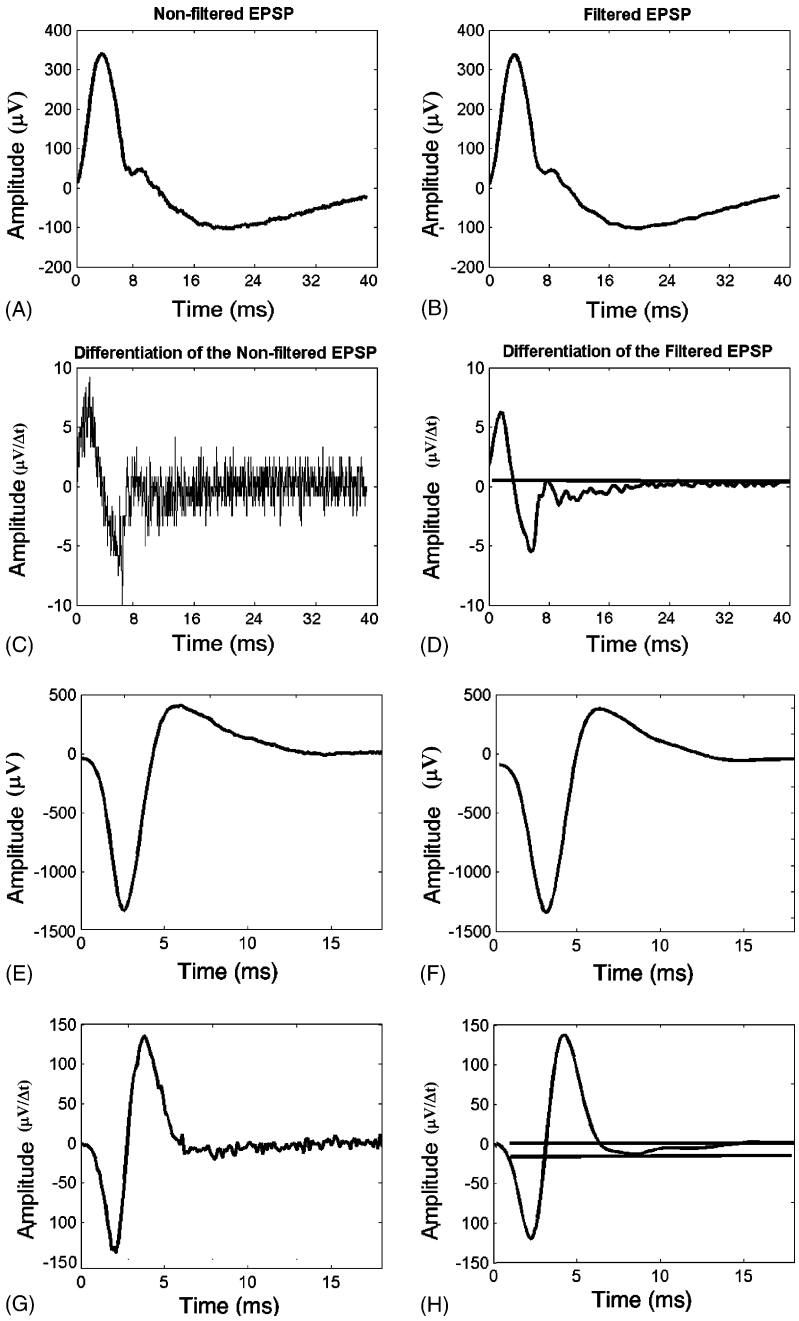

Fig. 6. The resulting differentiation of the filtered and non-filtered signal. (A) Non-filtered EPSP signal. (B) Filtered EPSP signal. (C) The result of the differentiation of the non-filtered EPSP signal. (D) The result of the differentiation of the filtered EPSP signal. (E) Non-filtered PS signal. (F) Filtered PS signal. (G) The result of the differentiation of the non-filtered PS signal. (H) The result of the differentiation of the filtered PS signal. It can be readily seen that the low pass filter is necessary in order to remove the high frequency noise that can be amplified during the differentiation phase.

PS case were set at $+14.52\,\mu$V/ms for θ_p and $-48.4\,\mu$V/ms for θ_n. These threshold values successfully distinguished the waveforms of interest from slow and noisy baseline activity. The application of the chosen threshold values to all EPSPs and PS in each RIT, across all RITs, defined a range of positive, negative, and transition duration intervals. Statistics of these intervals are shown on Table 1.

The output of the threshold function was integrated and the result was released by the decision function, if the set of positive and negative activity and transition duration criteria ($w_n > \omega_n$, $w_p > \omega_p$, and $w_{tr} > \omega_{tr}$) is met. The values for ω_n, ω_p, and ω_{tr} (Table 1) were chosen at 99% confidence bound using a right tail probability.

Finally, the scaling factor γ was calculated by averaging the ratio of the amplitude obtained through the classical method to the amplitude obtained through the proposed method. In the EPSP case, γ was found to be 1.001 (S.D. ± 0.002) while in the PS case, γ was found to be equal

Table 1
Average positive (w_p), negative (w_n), and transition (w_{tr}) duration for EPSPs and PSs, after applying the selected threshold values

	w_p (EPSP) (ms)	w_p (PS) (ms)	w_n (PS) (ms)	w_{tr} (PS) (ms)
RIT #1	3.89 (±0.40)	4.42 (±1.18)	3.37 (±1.25)	0.49 (±0.08)
RIT #2	3.84 (±0.41)	6.12 (±1.77)	4.71 (±2.29)	0.75 (±0.04)
RIT #3	3.18 (±0.34)	4.94 (±1.04)	3.49 (±1.0)	0.69 (±0.17)
RIT #4	2.85 (±0.29)	5.12 (±1.60)	3.69 (±1.58)	0.83 (±0.33)
RIT #5	3.46 (±0.33)	5.88 (±1.75)	3.33 (±1.61)	0.52 (±0.27)
Average	3.44 (±0.44)	5.29 (±0.70)	3.71 (±0.57)	0.66 (±0.14)
Threshold values	ω_p = 1.79	ω_p = 2.67	ω_n = 1.57	ω_{tr} = 0.14

The last row shows the interval threshold values for the decision function included in the intelligent integrator.

to 0.050 (S.D. ± 0.003). P is the length of the integration domain and it was set to 20 ms for both EPSP and PS.

Comparison between the amplitudes extracted by the classical and the proposed method provided an average eNMSE of 0.94% (S.D. ± 0.28%) for EPSPs and 2.48% (S.D. ± 1.73) for PSs. The small eNMSE values (<5%) suggested that for both EPSPs and PSs, the classical amplitude extraction method and the proposed amplitude extraction method yielded comparable results. The nonlinear dynamics were also preserved. In the case of EPSP, the first order kernel was overestimated by an average of 2.61% (S.D. ± 2.45%), while in the case of the PS it was overestimated by an average of 6.65% (S.D. ± 5.16%). Fig. 7A shows a representative second order kernel computed with the output dataset extracted with the classical method (gray) and the proposed method (black) in the case of EPSP. Fig. 8A shows a representative second order kernel computed with the output dataset extracted with the classical method (gray) and the proposed method (black) in the case of PS. In both cases, the second order kernels are very close in shape and size.

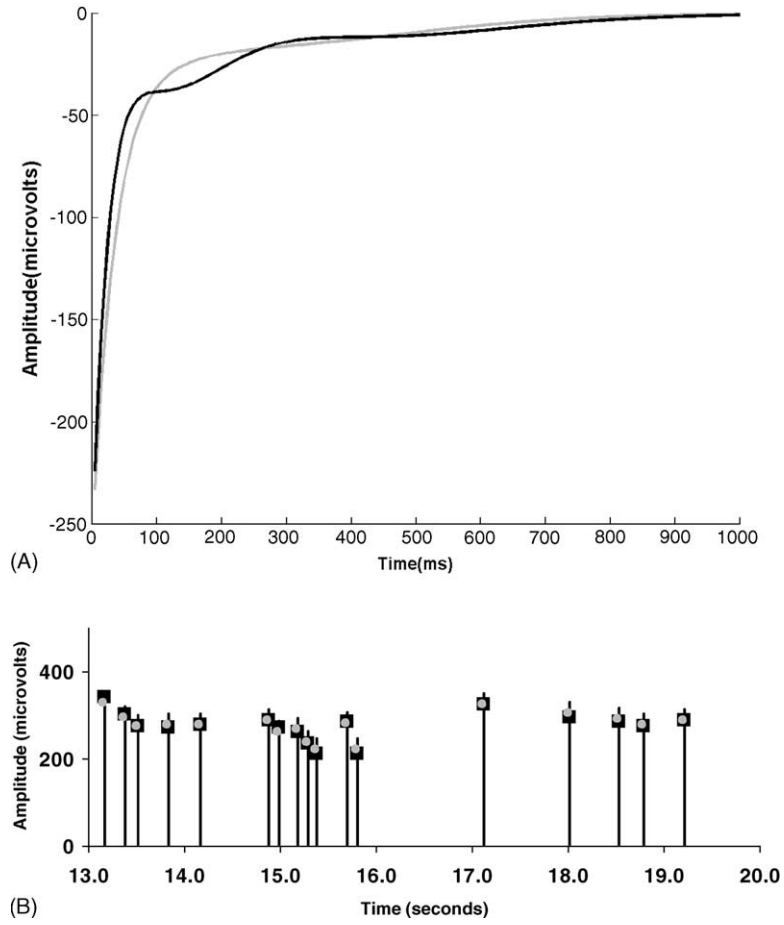

Fig. 7. (A) Second order kernels estimated from an EPSP classical dataset (gray curve) and an EPSP processed dataset (black curve). (B) Sample of EPSP amplitude extracted using the classic (gray circles) and the proposed method (black squares).

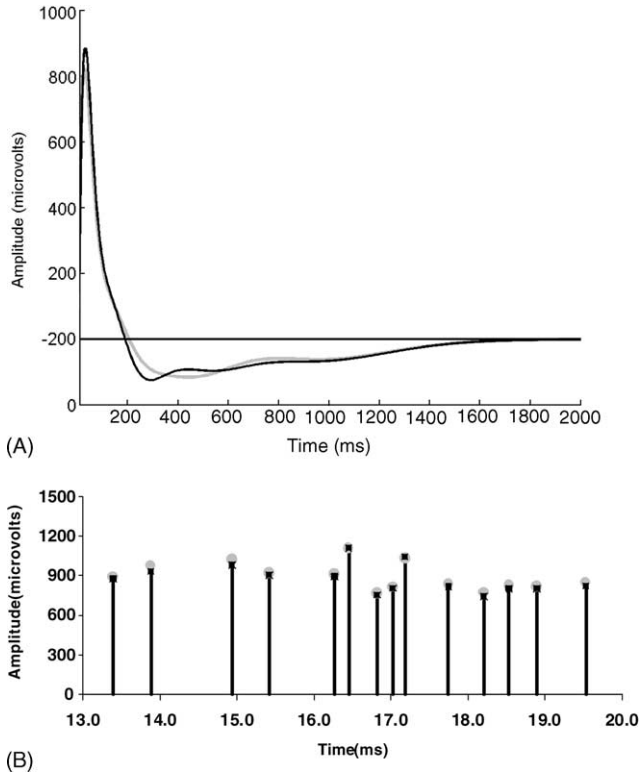

Fig. 8. (A) Second order kernels estimated from a PS classic dataset (gray curve) and a PS processed dataset (black curve). (B) Sample of population spike amplitude extracted using the classic (gray circles) and the proposed method (black squares).

A segment of an EPSP amplitude dataset extracted with the classical method (black) is compared to its counterpart extracted with the proposed method (gray) is shown in Fig. 7B. A segment of a PS amplitude dataset extracted with the classic method (black) is compared to its counterpart extracted with the proposed method (gray) is shown in Fig. 8B. In both figures, corresponding amplitudes extracted with the classical method (gray circles) and the proposed method (black squares) practically coincide. Similar conclusions were reached after evaluating the average prediction NMSE. In the case of EPSP, the average prediction NMSE (pNMSE) was 0.70% (S.D. $\pm$ 0.5%) when the classical amplitude extraction method was employed and 0.85% (S.D.$\pm$0.4%) when the proposed extraction method was employed. In the case of PS, the prediction NMSE (pNMSE) was 2.42% (S.D. $\pm$ 1.32%) when the classical amplitude extraction method was employed and 3.09% (S.D. $\pm$ 0.92%) when the proposed method was employed. The small pNMSE (<5%) values suggest high kernel and model accuracy. Table 2 and Table 3 summarize the results obtained from analyzing all five EPSP and the PS datasets respectively. Each row tabulates the results for each experiment. The last row shows the column averages. The columns of the tables include the values of eNMSE, k_1, and pNMSE used to compare extraction accuracy and preservation of nonlinear dynamics.

Table 2
Comparison between the classical and the proposed EPSP amplitude extraction method

	Extraction method	eNMSE (%)	k_1 (μV)	pNMSE (%)
RIT #1	Classic	0.67	294	1.10
	Proposed		294	1.18
RIT #2	Classic	0.74	390	1.44
	Proposed		405	1.30
RIT #3	Classic	0.80	165	0.44
	Proposed		162	0.44
RIT #4	Classic	1.17	212	0.18
	Proposed		208	0.51
RIT #5	Classic	1.3	105	0.33
	Proposed		97	0.83
Average	Classic	0.94 ($\pm$0.28)	232 ($\pm$111)	0.70 ($\pm$0.50)
	Proposed		233 ($\pm$119)	0.85 ($\pm$0.40)

In both cases, the small eNMSE values suggest that the proposed method extracts amplitude values almost identical to the classical method. The small pNMSE values and the small difference in pNMSE values between the two amplitude extraction methods, the small difference between the values of the first order kernels, and the close resemblance of the second order kernels, imply that the STP nonlinear dynamics were preserved regardless of whether the amplitude of the response field potential was extracted with the classical method or the proposed method. Therefore, the proposed method implements real time field potential amplitude extraction comparable to the amplitude extracted with the classical method preserving the system's nonlinear dynamic properties.

Finally, we examined the sensitivity of the proposed method to variations of the threshold values (θ_p and θ_n) in terms of the resulting eNMSE and pNMSE. Fig. 9A shows the plot of eNMSE versus increasing threshold values

Table 3
Comparison between the classical and the proposed PS amplitude extraction method

	Extraction method	eNMSE (%)	k_1 (μV)	pNMSE (%)
RIT#1	Classic	2.7	912	1.04
	Proposed		936	2.86
RIT#2	Classic	6	663	2.72
	Proposed		731	4.45
RIT#3	Classic	1.27	545	1.82
	Proposed		555	1.93
RIT#4	Classic	1.81	586	4.54
	Proposed		611	3.39
RIT#5	Classic	4.14	645	2.02
	Proposed		737	2.86
Average	Classic	2.48 ($\pm$1.73)	670 ($\pm$143)	2.42 ($\pm$1.32)
	Proposed		714 ($\pm$146)	3.09 ($\pm$0.92)

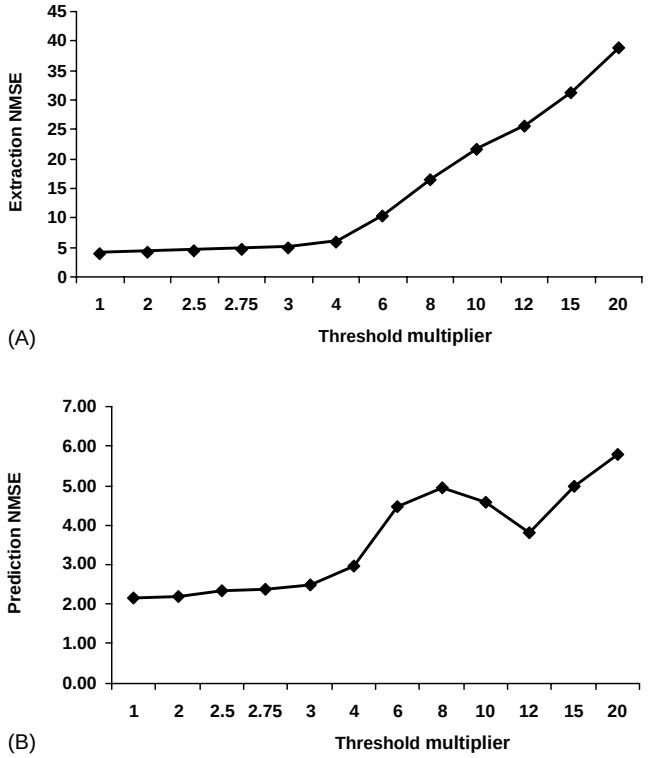

Fig. 9. Sensitivity analysis. (A) Plot of eNMSE vs. threshold level. (B) Plot of pNMSE vs. threshold level.

expressed as multiples of the selected threshold values. The pNMSE values were confined to the range of (3–5%) when the threshold value was less than four times the selected threshold values. Fig. 9B shows the plot of the pNMSE versus increasing threshold values expressed as multiples of the selected threshold values. The range of the pNMSE values increased from 3 to 4% to more than 6% as the threshold increased past four times the baseline value.

4. Discussion

New designs for biomedical devices such as portable medical equipment, biosensors, and neural prosthetics require new computational methods that can be integrated in hardware to extract in real time features of interest from inbound signals. To address this need in a new generation of SoC (System-on-a-Chip) based neuroprosthetic devices [Berger et al., 2001], we designed a new algorithm to extract the amplitude of neural field potentials, in particular, EPSP amplitudes and spike amplitudes. The proposed algorithm included a low pass filter, a differentiator, a threshold device, and an intelligent integrator. The low pass filter reduced the high frequency noise. The differentiator dissected the waveform into positive and negative domains. The threshold device clipped the undesirable part of the differentiated signal. The intelligent integrator computed the amplitude of valid EPSP or PS waveforms, qualified by the decision function. The proposed algorithm was implemented by tuning several parameters. The cutoff frequency selection for the LPF was based on the EPSP and PS power spectra. The adjustment of the threshold values (θ_p, θ_n) was based on the level of undesirable slow activity and residual noise. The decision function parameters (ω_n, ω_p, and ω_{tr}) were determined experimentally from five different experiments in each case.

The validation of the proposed algorithm with EPSP and population spike datasets recorded at the Dentate Gyrus and the CA1 hippocampus in vitro was successful. The accuracy of the amplitude extraction using the proposed method was very high as it was reflected in the extraction normalized mean square error (in the range of 2–4% for PSs and 0.6–1.3% for EPSPs). The STP nonlinear dynamics were also preserved as shown by the small difference between the value of the first order kernel computed using output amplitudes extracted with the classical method and the value of the first order kernel computed using output amplitudes extracted with the proposed method (Tables 2 and 3), and by the close resemblance of the second order kernels shown in Figs. 7A and 8A. The preservation of the STP nonlinear dynamics was also confirmed by the small pNMSE values (Tables 2 and 3).

The difference between the EPSP and the spike amplitude extraction was the choice of the threshold function and the parameters of the intelligent integrator. In the EPSP case, the output of the integrator corresponded to the peak EPSP amplitude. In the spike case, the output of the integrator corresponded to the average of the distance between the minimum and the first maximum in the population spike and the distance between the second peak and the minimum of the population spike. The implementation of this algorithm with electronics is focused on the use of field-programmable gate arrays (FPGAs). Implementation of the decision function with analog electronics could present several challenges, but FPGA implementations are much more accommodating with complex, real time logic.

Although the proposed field potential amplitude extraction method was validated with EPSP and PS waveforms from the hippocampus, it is readily applicable to other types of evoked potentials such as sensorimotor evoked potentials, auditory evoked potentials, visual evoked potentials, and various forms of spike activity, by using the following steps as a guideline: (1) record a few field potential responses, (2) use the power spectra to determine the cutoff frequency for the LPF, (3) determine the thresholds (θ_p and θ_n) from the differentiated signal, (4) compute positive phase, negative phase and transition interval thresholds (ω_n, ω_p, and ω_{tr}), (5) evaluate extraction accuracy via eNMSE and preservation of the system's nonlinear dynamic properties via, pNMSE and the computed kernels.

Acknowledgements

This work was supported by Grant No. RR-01861 from the Division of Research Resources of the National

Institutes of Health and by Grants 0646 and 0259 from DARPA Controlled Biological Systems Program and the Office of Naval Research.

References

Anderson WW, Collingridge GL. The LTP Program: a data acquisition program for on-line analysis of long-term potentiation and other synaptic events. J Neurosci Methods 2001;108:71–83.

Berger TW, Baudry M, Brinton RD, Liaw JS, Marmarelis VZ, Park AY, et al. Brain-implantable biomimetic electronics as the next era in neural prosthetics. Proc IEEE 2001;89(7):993–1012 [Special Issue SI July].

Colletti V, Fiorino F, Policante Z, Bruni L. Intraoperative monitoring of facial nerve antidromic potentials during acoustic neuroma surgery. Acta Oto-Laryngologica 1997;117(5):663–9.

Courellis SH, Marmarelis VZ, Berger TW. Modeling event-driven nonlinear dynamics in neuronal systems with multiple inputs. Seattle, WA: Annual Conference Biomedical Engineering Society; 2000.

Donoghue JP. Connecting cortex to machines: recent advances in brain interfaces. Nat Neurosci 2002;5:1085–8 [Suppl. S, November].

Gholmieh G, Soussou W, Courellis S, Marmarelis VZ, Berger TW, Baudry M. A biosensor for detecting changes in cognitive processing based on nonlinear systems analysis. Biosens Bioelectron 2001;16(7–8):491–501.

Gholmieh G, Courellis S, Marmarelis VZ, Berger TW. A novel method for modeling short-term synaptic plasticity. J Neurosci Methods 2002;21(2):111–27.

Gross GW, Rhoadas BK, Reust DL, Schwalm RC. Stimulation of monolayer networks in culture through thin film indium-tin oxide recording electrodes. J Neurosci Methods 1993;50:131–43.

Han M, Gholmieh G, Soussou W, Berger TW, Tanguay Jr AR. Conformally-mapped multielectrode arrays for in-vitro stimulation and recording of hippocampal acute slices. In: Proceedings of the Second Joint IEEE Engineering in Medicine and Biology Society and the Biomedical Engineering Society Conference, Houston, TX, 2002, p. 2127–28.

Hedwig B, Knepper M. Separation of synaptic and spike activity in intracellular recordings for selective analysis. J Neurosci Methods 1992;42(1–2):83–90.

Johnston D, Wu SM. Extracellur field recordings. In: Foundations of cellular neurophysiology. MIT Press; 1995.

Lagmoen IA, Andersen P. The hippocampal slice in vitro. A description of the technique and some examples of the opportunities it offers. In: Electrophysiology of isolated mammalian CNS preparations. London: Academic Press; 1981. p. 51–105.

Pesaran B, Pezaris JS, Sahani M, Mitra PP, Andersen RA. Temporal structure in neuronal activity during working memory in macaque parietal cortex. Nature Neurosci 2002;5(8):805–11.

Stecker MM, Cheung AT, Patterson T, Savino JS, Weiss SJ, Richards RM, et al. Detection of stroke during cardiac operations with somatosensory evoked responses. J Thoracic Cardiovasc Surgery 1996;112(4):962–72.

Stoppini L, Duport S, Correges P. A new extracellular multirecording system for electrophysiological studies: application to hippocampal organotypic cultures. J Neurosci Methods 1997;72(1):23–33.

Thiebaud P, de Rooij NF, Koudelka-Hep M, Stoppini L. Microelectrode arrays for electrophysiological monitoring of hippocampal organotypic slice cultures. IEEE Trans Biomed Eng 1997;44(11):1159–63.

Xie X, Berger TW, Barrionuevo G. Isolated NMDA receptor-mediated synaptic responses express both LTP and LTD. J Neurophysiol 1992;67(4):1009–13.

Zaaroor M, Pratt H, Feinsod M, Schacham SE. Real-time monitoring of visual evoked potentials. Isr J Med Sci 1993;29(1):17–22.